*Journal of The Electrochemical Society*, **159** (5) G56-G61 (2012)
0013-4651/2012/159(5)/G56/6/$28.00 © The Electrochemical Society

# Low-k $SiC_xN_y$ Films Prepared by Plasma-Enhanced Chemical Vapor Deposition Using 1,3,5-trimethyl-1,3, 5-trivinylcyclotrisilazane Precursor

**Hung-En Tu, Yu-Han Chen, and Jihperng Leu**[*,z]

*Department of Materials Science and Engineering, National Chiao Tung University, Hsinchu 30049, Taiwan*

Low-k silicon carbonitride ($SiC_xN_y$) films with k of 3.6–4.6 were prepared by radio frequency plasma-enhanced chemical vapor deposition at 25 to 400°C under low power density of 0.15 W/cm$^3$, using a single source precursor, 1, 3, 5-trimethyl-1, 3, 5-trivinylcyclotrisilazane (VSZ), and Ar. At lower deposition temperatures ($\leq$ 200°C), most cyclic VSZ structures were preserved in the $SiC_xN_y$ films, resulting in a lower density (1.60–1.76 g/cm$^3$), a lower dielectric constant (k$\sim$3.6–3.9) and a fairly good elastic modulus of 22.0–25.0 GPa. When the deposition temperature was raised to 400°C, the cyclic N-Si-N linkages were reformed to a dense Si-N structure, with the desorption of $CH_x$ bonds, resulting in higher density (2.0 g/cm$^3$), a dielectric constant of 4.6, and an excellent elastic modulus of 65.2 GPa. The leakage current density of $SiC_xN_y$ films was reduced from $1.5\times10^{-6}$ to $4.0\times10^{-8}$ A/cm$^2$ at 1 MV/cm, upon increasing the deposition temperature from 25°C to 400°C. The conduction mechanism of the $SiC_xN_y$ films, except the film deposited at 400°C and tested under higher electric field, exhibited Schottky emission due to few charged defects by using a cyclic VSZ precursor and a lower plasma power density of 0.15 W/cm$^3$.
© 2012 The Electrochemical Society. [DOI: 10.1149/2.085205jes] All rights reserved.

Manuscript submitted December 7, 2011; revised manuscript received February 14, 2012. Published March 2, 2012.

As the dimensions of integrated circuits are scaled according to Moore's law, the increase in propagation (RC) delay, crosstalk noise and power dissipation in the backend interconnects become the limiting factors in the ultra-large scale integrated devices.[1] To reduce the capacitance in the backend interconnects, low dielectric constant (k < 3.5) material was first introduced as an interlayer dielectric (ILD).[2] Meanwhile, silicon nitride was retained as the etch-stop and diffusion barrier layer in the dual damascene architecture, because of its excellent etch selectivity and barrier effectiveness, although its dielectric constant is relatively high, at 6.5–7.0.[3] In order to further reduce the capacitance in the backend interconnects, the semiconductor industry has consistently tried to achieve lower effective dielectric constants, which involves low-k ILD and low-k etch-stop layer with reduced thickness.[4,5]

To reduce the k-value of silicon nitride films, silicon carbonitride ($SiC_xN_y$) thin films have been introduced as an etch stop/barrier layer,[6–8] because of their low dielectric constant and their properties as effective barriers against Cu diffusion and drift.[9,10] In addition to sputtering deposition and laser vapor deposition methods, silicon carbonitride films have been prepared by plasma-enhanced chemical vapor deposition (PECVD), using multi-precursors such as $SiH_4$+$NH_3$($N_2$)+$CH_4$[11,12] and $SiH(CH_3)_3$ +$NH_3$.[8,13,14] In recent years, single source precursors, such as hexamethyldisilazane (HMDS), for low-k $SiC_xN_y$ applications,[9,15] and tris(dimethylamino)silane[16] and 1,3-bis(dimethylsilyl)-2,2,4,4-tetramethylcyclo- disilazane,[10] for increased mechanical and tribological performance, have been the subject of much research, because they retain the ready fragments and allow better control of the composition of films, compared to multi-precursors.

In this paper, a new, cyclic organosilazane, 1, 3, 5-trimethyl-1, 3, 5-trivinyl- cyclotrisilazane (VSZ) with a cyclic Si-N-Si, pendent $CH_3$, and vinyl groups, as illustrated in Figure 1, is used as a single source precursor for the deposition of low-k $SiC_xN_y$ films by the radio frequency (RF) PECVD technique using a low power density (0.15 W/cm$^3$). This approach may allow the retention of most of the chemical bondings, such as the pendent Si-$CH_3$ for low polarazability and the use of cyclic Si-N-Si in the starting precursor to reduce the dielectric constant, while maintaining fairly good mechanical strength when the vinyl groups in single source precursor are broken to form a cross-linked structure.[17] This study used Fourier transform infrared spectroscopy (FTIR) and X-ray photoelectron spectroscopy (XPS) to investigate the effect of deposition temperature on the chemical structure of low-k $SiC_xN_y$ films. In addition, the films' properties and electric characteristics, such as density, elastic modulus, dielectric constant, dielectric breakdown and leakage behavior were also studied.

## Experimental

The $SiC_xN_y$ films were deposited onto (100) silicon wafers by a RF (13.56 MHz) parallel-plate PECVD system, in which the electrode spacing and the diameter of the electrode were 20 and 150 mm, respectively. 1, 3, 5-trimethyl-1, 3, 5- trivinylcyclotrisilazane ($C_9H_{21}N_3Si_3$, VSZ) (Gelest, Inc. 95%) was used as the single source precursor. The liquid precursor was vaporized at 60°C, to prevent condensation, and carried to the reactor using an argon carrier gas at a flow rate of 20 sccm. The showerhead in the upper electrode distributed the precursor and gases uniformly over the substrate. The deposition pressure and RF power were maintained at 90 mTorr and 50 W (power density = 0.15 W/cm$^3$), respectively, without bias. The deposition temperatures were varied from room temperature to 400°C, to investigate the influence of deposition temperature on the structures and properties of $SiC_xN_y$ films.

The chemical bonding and composition of $SiC_xN_y$ films were examined using specular reflectance FTIR (MAGNA-IR Technology Protege 460) at a 50° incident angle. The FTIR spectra were collected in the 500–4000 cm$^{-1}$ range at a resolution of 4 cm$^{-1}$, with a total of 32 scans.

XPS analyzes were performed, to examine the chemical bonding and compositions, using a PHI Quantera AES 650) with a monochromated Al $k_\alpha$ X-ray source (h$\nu$ = 1486.6 eV) with an energy resolution of 0.1 eV. The surface of the specimen was pre-cleaned by bombardment with $Ar^+$ ions (5 kV), prior to the collection of XPS data. A neutral gun was employed, to eliminate the charge effect during the XPS measurement. The XPS spectrum was calibrated by the binding energy of the Au $4f_{7/2}$ line at 84.0 eV. Quantification of XPS data was achieved using peak areas and experimental sensitivity factors.

Nanoindentation tests were carried out using a nanoindentor (MTS Nano Indenter XP System) with a Berkovich tip, in continuous mode, to obtain the reduced modulus ($E_r$). The Oliver–Pharr method[18] was then used to determine the elastic modulus (E) of various $SiC_xN_y$ films. To eliminate the effect of the Si substrate, the indentation depth was maintained at less than 20% of the film's thickness. The density of the $SiC_xN_y$ film was measured by X-ray reflectivity (XRR) (Bruker D8 Discover), with a Cu $K_\alpha$ source ($\lambda$ = 0.154 nm), using $\omega$-2$\theta$ scan mode. The scanning region ranged from 0° to 2°. The XRR data was

* Electrochemical Society Active Member.
z E-mail: jimleu@mail.nctu.edu.tw

Downloaded on 2014-04-28 to IP 140.113.38.11 address. Redistribution subject to ECS terms of use (see ecsdl.org/site/terms_use) unless CC License in place (see abstract).

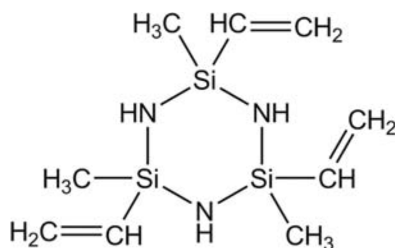


**Figure 1.** Structure of liquid precursor, VSZ.

analyzed by LEPTOS simulation software, to fit the density of $SiC_xN_y$ film.

The dielectric constant (k) and leakage current of the $SiC_xN_y$ films were characterized by capacitance-voltage (C-V) (HP 4280) measurement and current-voltage (I-V) measurement, using metal-insulator-semiconductor (MIS) structure configuration [Al electrode/$SiC_xN_y$ film/Si (50 ohm-cm)] at room temperature. To accurately measure the dielectric constant by C–V dot measurement, three circular aluminum dots of nominal diameters 200, 400, and 800 mm were used, to minimize the geometric effect. Aluminum electrodes with a thickness of 1 μm were coated onto the dielectric films by ULVAC EBX-6D thermal evaporator through a shadow mask. Measurements of film thickness were made using an n&k Analyzer 1280 (n&k Technology, Inc.) at wavelengths ranging from 190 to 900 nm. The I-V characteristics were measured at room temperature, under $N_2$ purge, using a HP 4156B with a diameter of 200 μm as the electrode. For C-V and I-V measurement, the thickness of the $SiC_xN_y$ films was between 100 and 130 nm. For nanoindentation measurement, a nominal thickness of 1 μm was used, to avoid the substrate effect.

## Results and Discussion

*Infrared and XPS analysis of PECVD films.—* The chemical bonding types in the PECVD $SiC_xN_y$ films prepared at various substrate temperatures were first characterized by specular reflectance FTIR spectroscopy. Figure 2 shows the FTIR spectra of the starting liquid precursor, VSZ and the PECVD $SiC_xN_y$ thin films, deposited at various substrate temperatures. The characteristic features of the infrared spectrum of VSZ precursor included Si-N, Si-C, $CH_3$, $CH_2$, C=C and N-H bonding types, as summarized in Table I. The primary absorption bands at 922 and 1048 $cm^{-1}$ corresponded to the asymmetric stretching vibration modes of the Si-N bond of the cyclic Si-N-Si structure. Si-$CH_3$ bonding includes the stretching vibration of the Si-C bond at 800 $cm^{-1}$,[9,10,15] the bending vibration of the Si-$CH_3$ bonds at 1265 $cm^{-1}$[9,10,15] and the asymmetric stretching vibration of the C-$H_3$ bond at 2964 $cm^{-1}$.[10,15,17] Other bonding included the stretching vibration of the C=C bonds of Si-CH=$CH_2$ at 1600 $cm^{-1}$,[17,19] the asymmetric stretching vibration of the $CH_2$ bond in the vinyl group at 3055 $cm^{-1}$,[15,17,19] the bending vibration of the $CH_2$ bond in the vinyl group at 1409 $cm^{-1}$,[15,17,19] and the stretching vibration of the N-H bond at 3370 $cm^{-1}$[20] and the N–H bending mode at 1180 $cm^{-1}$.[15,20]

Table I. Identification of IR absorption bands in VSZ and $SiC_xN_y$ films. ν = stretching, δ = bending, a = asymmetric, s = symmetric vibration, and Me=$CH_3$.

| Absorption band ($cm^{-1}$) | | | |
|---|---|---|---|
| VSZ | $SiC_xN_y$ (400°C) | Attributed Sources | References |
| 800 | | ν Si-C | 9, 10, 15 |
| 1265 | 1265 | δ $SiMe_n$ (n = 1 or 2) | 9, 10, 15 |
| 922, 1048 | 922, 1038 | $\nu_a$ Si-N-Si | 10 |
| 1180 | 1150 | δ N-H in Si-NH-Si | 15, 20 |
| 1600 | | ν C=C | 17, 19 |
| | 1625 | ν CN-H | 21 |
| | 2100–2200 | ν Si-H or C-N | 10, 15, 22 |
| 2964 | 2887, 2956 | $\nu_s$ $CH_3$, $\nu_a$ $CH_3$ | 10, 15, 17, 19 |
| | 2910 | $\nu_a$ $CH_2$ | 17 |
| 3055, 1409 | | $\nu_a$ $CH_2$, δ $CH_2$ in vinyl group | 15, 17, 19 |
| 3370 | 3370 | ν N-H | 20 |

Upon plasma deposition, significant changes were observed in the infrared spectrum of the $SiC_xN_y$ film deposited at room temperature. The major absorption bands of VSZ and a representative $SiC_xN_y$ film, and their attributed sources are summarized in Table I. The absorption bands related to Si-N at 922 and 1038 $cm^{-1}$ remain the strongest bands. The absorption bands for the C=C at 1600 $cm^{-1}$ and the $CH_2$ bonds in the vinyl groups at 3055 $cm^{-1}$ and 1409 $cm^{-1}$ disappeared. In contrast, the asymmetric $CH_2$ and symmetric $CH_3$ stretching vibrations at 2910 and 2887 $cm^{-1}$ appeared.[10,15,17,19] Also, the broad N-H bands at 3370 $cm^{-1}$ and 1150 $cm^{-1}$ appeared with enhanced intensities.[20,21] There was a minor loss in the Si-$CH_3$ band at 1265 $cm^{-1}$ and the C-$H_3$ absorption band at 2956 $cm^{-1}$, due to chain scission of Si-$CH_3$ under plasma conditions. These results showed that most of the cyclic N-Si-N linkages were preserved in the $SiC_xN_y$ films after the PECVD process. Some of the cyclic N-Si-N bonds were broken, which resulted in an increase in the formation of Si-N-H and C-NH bonds. The reactive C=C bonds of the vinyl group were broken to form a cross-linked structure, during the plasma deposition process, which is similar to that reported by Lubguban et al. for low-k organosilicate glass using tetravinyltetramethylcyclotetrasiloxane precursor.[17] The hypothesis is supported by the appearance of $CH_2$ vibration modes at 2910 (asym. $CH_2$), related to Si-$(CH_2)_n$-Si (n = 1 or 2), after the breaking of the vinyl groups. These are indicators of the cross-linked structure. The other reaction path formed a terminal Si-$CH_2$-$CH_3$, which may be further broken up into Si-$CH_3$ and Si-H.

As the deposition temperature was raised to ≥100°C, the absorption intensity of Si-N-Si continued to increase, up to 400°C, with its absorption band shifting from ∼1048 $cm^{-1}$, at a deposition temperature of 25°C, to the lower wavenumber, 1038 $cm^{-1}$, for a deposition temperature of 400°C. In contrast, the C=C bond at 1600 $cm^{-1}$ and the -$CH_2$ asymmetric stretching associated with the vinyl group at 3055 $cm^{-1}$ disappeared, as illustrated in Figure 2. The intensities of

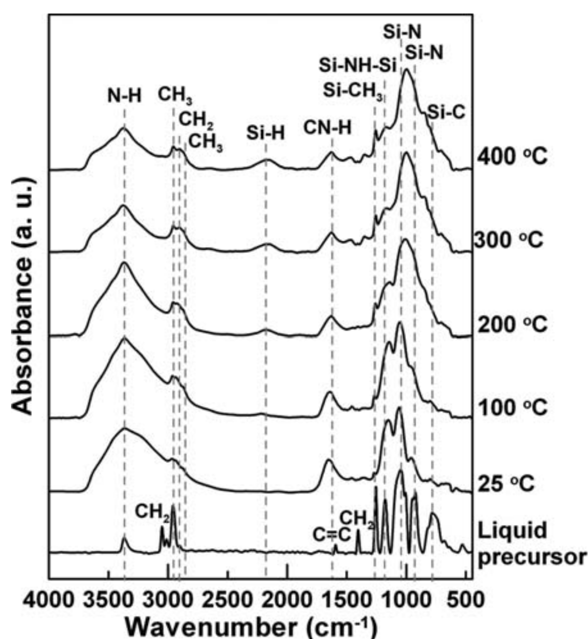


**Figure 2.** FTIR spectra of the VSZ liquid precursor and $SiC_xN_y$ films deposited at various deposition temperatures.

Downloaded on 2014-04-28 to IP 140.113.38.11 address. Redistribution subject to ECS terms of use (see ecsdl.org/site/terms_use) unless CC License in place (see abstract).

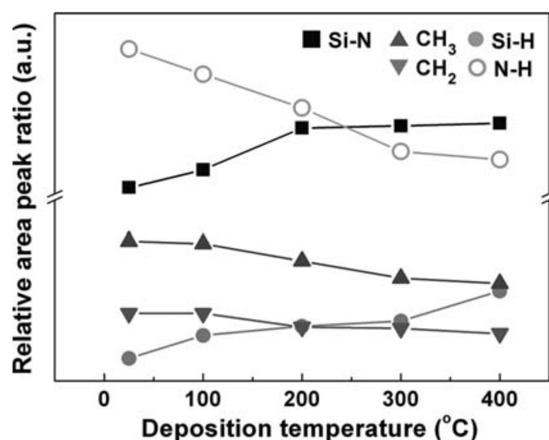


**Figure 3.** The relative peak ratios of Si-N, C=C, $CH_x$, and N-H infrared absorption bands in the $SiC_xN_y$ films as a function of deposition temperature.

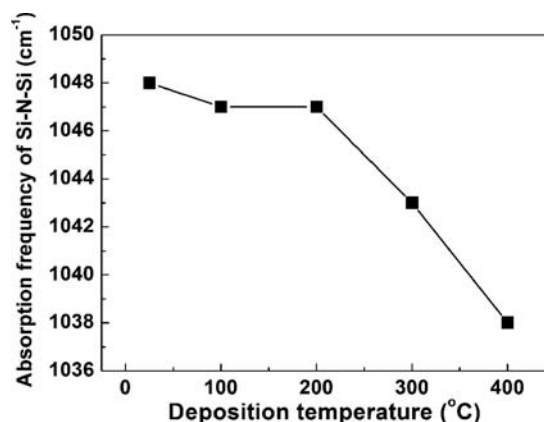


**Figure 4.** The absorption frequency of Si-N-Si as a function of deposition temperature.

the Si-$CH_3$ band at 1265 $cm^{-1}$ and the N-H bands at 3370 $cm^{-1}$ and 1150 $cm^{-1}$ (1625 $cm^{-1}$ CN-H) decreased, as deposition temperature was increased, presumably due to the formation of volatile $CH_4$ or $NH_3$. A new absorption peak, for Si-H[10,15] or C-N[22] at around 2100 $cm^{-1}$ became visible at T $\geq$200°C and increased, as deposition temperature was increased. The formation of Si-H was a result of the N-Si-N scission and reaction with hydrogen radicals from the plasma processes, while the C=C bonds of the vinyl groups were broken and attached to the fragments of N-H to form C-NH.

The quantitative change in the Si-N, N-H, $CH_3$, $CH_2$, and Si-H bonds in the $SiC_xN_y$ films as a function of deposition temperature is shown in Figure 3, based on the area ratio of their respective infrared absorption bands, shown in Figure 2. As deposition temperature was increased, the ratio of the Si-N bonds increased and reached a plateau at T $\geq$ 200°C, while the ratio of Si-H bonds increased linearly, as deposition temperature increased. In contrast, the ratio of N-H (3300, 1150 $cm^{-1}$) and $CH_3$ decreased approximately linearly, as deposition temperature was increased, because the labile $CH_3$ bonds were more volatile at higher deposition temperatures. Also, the formation of $CH_2$ in Si-CH=$CH_2$ and $CH_2$ in Si-$(CH_2)_n$-Si, Si-$CH_2$-$CH_3$ or Si-$CH_2$-CNH showed a decreasing trend at deposition temperatures >25°C. This result showed that the Si-CH=$CH_2$ of the vinyl groups were broken to react with another vinyl group, forming Si-$(CH_2)_n$-Si and C-N bonds, during the PECVD process. Simultaneously, the absorption intensity of the Si-H bond increased, as deposition temperature was increased.[23]

In addition to infrared analysis, the compositions of $SiC_xN_y$ films deposited at various deposition temperatures and their relative ratios to Si were quantified by XPS. These are summarized in Table II. For reference, the ideal elemental compositions of the VSZ precursor were 20% Si, 60% C and 20% N, i.e. C/Si ratio = 3 and N/Si ratio = 1. When depositing $SiC_xN_y$ film at room temperature, the C/Si and N/Si ratios were 1.8 and 0.46, which were less than those of the VSZ precursor, at 3.0 and 1.0, respectively. The reduction in the C/Si and N/Si ratios of PECVD film deposited at room temperature indicated that the cyclic structure of the Si-N-Si bonds and the branches of Si-$CH_3$ bonds were broken up to some degree, during plasma processing. In addition, the ablation of C and N relative to Si probably occurred due to the formation of volatile $CH_4$ and $NH_3$ by-products during the plasma deposition process.

**Table II. Compositions of $SiC_xN_y$ films deposited at various deposition temperatures.**

| Deposition temperature, °C | Composition, at.% (ratio relative to Si) | | |
|---|---|---|---|
| | Si | C | N |
| 25 | 30.5 (1) | 55.5 (1.82) | 14.0 (0.46) |
| 100 | 48.6 (1) | 39.5 (0.81) | 11.9 (0.25) |
| 200 | 49.0 (1) | 39.2 (0.80) | 11.8 (0.24) |
| 300 | 51.3 (1) | 37.0 (0.72) | 11.7 (0.23) |
| 400 | 65.8 (1) | 19.3 (0.29) | 14.9 (0.23) |

The N/Si ratio of the $SiC_xN_y$ films decreased from 0.46 at 25°C to 0.25–0.23 for deposition temperature between 100°C and 400°C. In contrast, their respective C/Si ratio decreased from 0.86 at 25°C to 0.7-0.81 at T ~100–300°C and then there was a more radical decrease to 0.29 at a deposition temperature of 400°C. This implied that during the deposition of $SiC_xN_y$ film at 400°C by PECVD, the desorption of $CH_x$ bonds may occur simultaneously, due to a pyrolysis process, which resulted in the rearrangement of the films' structure and the subsequent formation of dense $SiC_xN_y$ films.[23] In addition to the XPS results, Figure 4 shows the position of the absorption band of N-Si-N in $SiC_xN_y$ films deposited by PECVD at various temperatures, as measured by FT-IR analysis. At temperatures $\leq$200°C, the Si-N absorption band was centered at 1047–1048 $cm^{-1}$ and still displayed the characteristics of cyclic N-Si-N. As the deposition temperature was raised to 300 and then 400°C, the Si-N absorption band was downshifted to 1043 and 1038 $cm^{-1}$, respectively. This redshift implied that the cyclic N-Si-N structures were broken up and reformed to a dense Si-N structure.[24]

*Properties of PECVD films.*— Film density is an important physical property of $SiC_xN_y$ films and is sensitive to free volume and cross-linked structure. Figure 5 shows the density of the $SiC_xN_y$ films as a function of deposition temperature. The densities of the $SiC_xN_y$ films increased monotonically, from 1.6, 1.67, 1.76, 1.83 to 2.0 g/$cm^3$, as deposition temperature increased through 25, 100, 200, 300, to 400°C. According to IR and XPS results, the intensities of the $CH_x$ bonds and the Si-C/Si-N ratio for the films decreased with increasing deposition temperature. The carbon content of the $SiC_xN_y$ films also decreased, as deposition temperature increased. The cyclic N-Si-N structures were broken up and reformed into a dense Si-N structure,[24] based on the redshift in the Si-N absorption (Fig. 4), as described in the previous section. Therefore, a rise in deposition temperature caused the scission of Si-$CH_2CH_3$ or Si-$CH_3$ bonds into Si-H bonds, which reduced the surrounding free volume in the $SiC_xN_y$ films.[25] The free radical species created by the scissile vinyl groups in the VSZ structure were rearranged with a backbone structure to form cross-linked, dense $SiC_xN_y$ films, which resulted in an increase in the films' density at higher deposition temperatures.

Figure 6 shows the elastic modulus of the $SiC_xN_y$ films as a function of deposition temperature. The elastic moduli varied from 21.0 GPa to 65.2 GPa, as the deposition temperature was increased

Downloaded on 2014-04-28 to IP 140.113.38.11 address. Redistribution subject to ECS terms of use (see ecsdl.org/site/terms_use) unless CC License in place (see abstract).

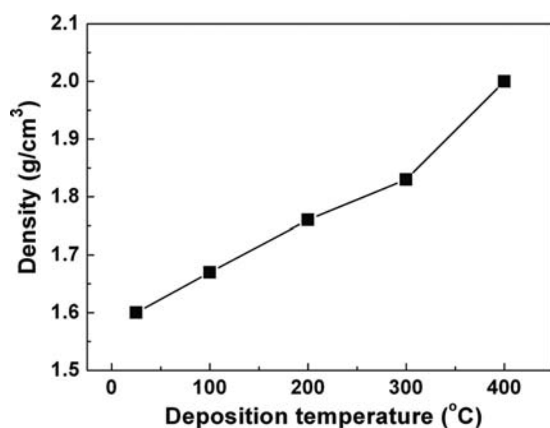


**Figure 5.** The density of the $SiC_xN_y$ films as a function of deposition temperature.

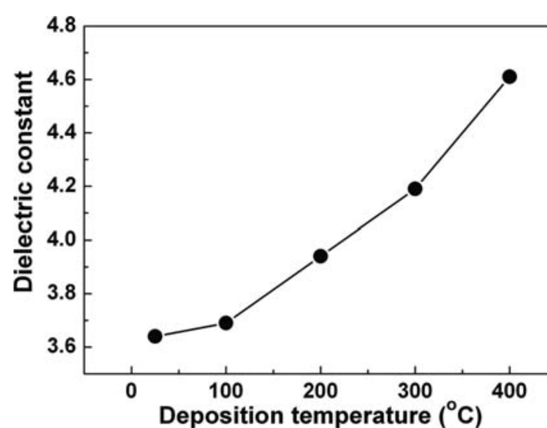


**Figure 7.** The dielectric constant of the $SiC_xN_y$ films as a function of deposition temperature.

from 25°C to 400°C. As deposition temperature was increased, the elastic modulus of the $SiC_xN_y$ films increased linearly, due to the scission of the Si-N-Si linkages and the desorption of $CH_x$ bonds to increase the crosslinked structure, as confirmed by FTIR. The highest values for the elastic modulus and hardness, obtained at 400°C, were 65.2 GPa and 6.5 GPa, respectively. This result showed that the hardness and elastic modulus of $SiC_xN_y$ films at lower deposition temperatures, using the VSZ precursor, were higher than those for the $SiC_xN_y$ films (H = ~1.9 GPa, E = ~12.2 GPa) using HMDS[9] as the single source precursor. Thus, for $SiC_xN_y$ films using a single source precursor, the VSZ precursor yielded a better mechanical strength than HMDS, primarily due to the fact that its vinyl groups were reformed to a cross-linked structure, under PECVD deposition conditions.

*Dielectric constant and leakage behavior.—* Figure 7 shows the dielectric constant of the $SiC_xN_y$ films as a function of deposition temperature. As deposition temperature was increased, the dielectric constant of the $SiC_xN_y$ films increased from 3.6 to 4.6. The scission the Si-C bonds, accompanied by a decrease in carbon content, were observed at higher deposition temperatures. This inverse relationship between the concentration of carbon and the dielectric constant is in agreement with the findings of other reports.[17,26] In addition, the reduced free volume of the $SiC_xN_y$ films, due to the formation of bonding such as Si-H and the formation of cross-linked Si-N structures at higher temperatures, contributed to an increase in not only the dielectric constant, but also in mechanical properties such as the elastic modulus.

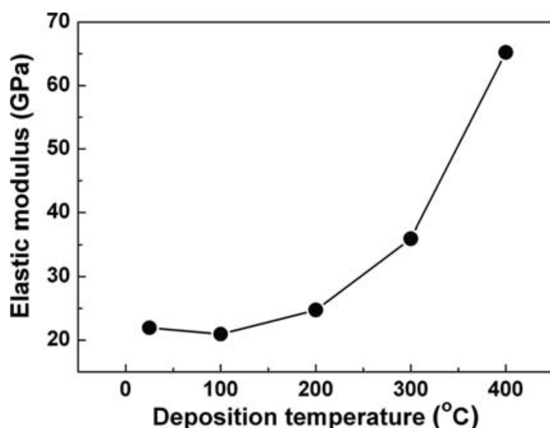


**Figure 6.** Elastic modulus of the $SiC_xN_y$ films as a function of deposition temperature.

Figure 8a shows the leakage current density as a function of the electric field for $SiC_xN_y$ films deposited at various deposition temperatures. The leakage current density showed a decreasing trend from $1.5\times10^{-6}$ to $4.0\times10^{-8}$ A/cm$^2$ at 1 MV/cm, as deposition temperature increased. Their breakdown strengths were all >3 MV/cm. A lower leakage current density was obtained at deposition temperatures $\geq$ 300°C. This can be attributed to a decrease in pendent $CH_3$ and an increase in more stable Si-N bonding, as verified by the XPS results, which showed a decreasing Si-C/Si-N ratio as deposition temperature was increased. Moreover, the $SiC_xN_y$ films became denser at higher deposition temperatures, which reduced the carrier transport and leakage current in $SiC_xN_y$ films.[14,27]

The conduction mechanism for leakage current is presumably attributed to the Schottky emission (SE) mechanism, which was induced by thermionic emission across the potential energy barrier at a metal-insulator interface, for $SiC_xN_y$ films deposited at $\leq$300°C. The current density of the SE mechanism is expressed by the following Eq. 1:[28]

$$J = A^* T^2 \exp\left(\frac{\beta_s E^{1/2} - \phi_s}{k_B T}\right) \quad [1]$$

where $\beta_s = (e^3/4\pi\varepsilon_0\varepsilon)^{1/2}$, $e$ is the electronic charge, $\varepsilon_0$ is the dielectric constant of free space, $\varepsilon$ is the relative dielectric constant, $A^*$ is the Richardson constant, $E$ is the applied electric field, $\phi_s$ is the contact potential barrier, $T$ is the temperature, and $k_B$ is the Boltzmann constant. The SE mechanism was confirmed by the linear correlation between ln(J/T$^2$) and E$^{1/2}$,[29] for films deposited at 25–300°C as shown in Figs. 8b–8e. It is believed that silicon dangling bonds in $SiC_xN_y$ films create states in the energy band-gap and are responsible for hopping conduction, as proposed by Robertson and Powell.[30]

Figure 9a shows the leakage current versus the average electric field plot for $SiC_xN_y$ film deposited at 400°C. The result suggested that the current conduction mechanism changed from the SE mechanism in the low field to the Frenkel-Poole (F-P) emission mechanism in the high field (>2.0 MV/cm). The current density in the F-P emission mechanism is expressed by the following Eq. 2:[28]

$$J = J_0 \exp\left(\frac{\beta_{PF} E^{1/2} - \phi_{PF}}{k_B T}\right) \quad [2]$$

where $J_0 = \sigma_0 E$ is the low-field current density, $\sigma_0$ is the low-field conductivity, $\beta_{PF} = (e^3/\pi\varepsilon_0\varepsilon)^{1/2}$ and $\phi_{PF}$ is the energy barrier height of the trap level. The F-P emission mechanism was confirmed by the linear relationship between ln(J/E) versus to E$^{1/2}$[29] for the electric field ranging from 2.0 to 3.0 MV/cm, as shown in Figure 9b. In the F-P emission mechanism, charge transport was dominated by the carriers that were captured and emitted by charged traps with coulomb potentials. These results indicated that charged defects existed in the the low-k $SiC_xN_y$ film deposited at 400°C.

Downloaded on 2014-04-28 to IP 140.113.38.11 address. Redistribution subject to ECS terms of use (see ecsdl.org/site/terms_use) unless CC License in place (see abstract).

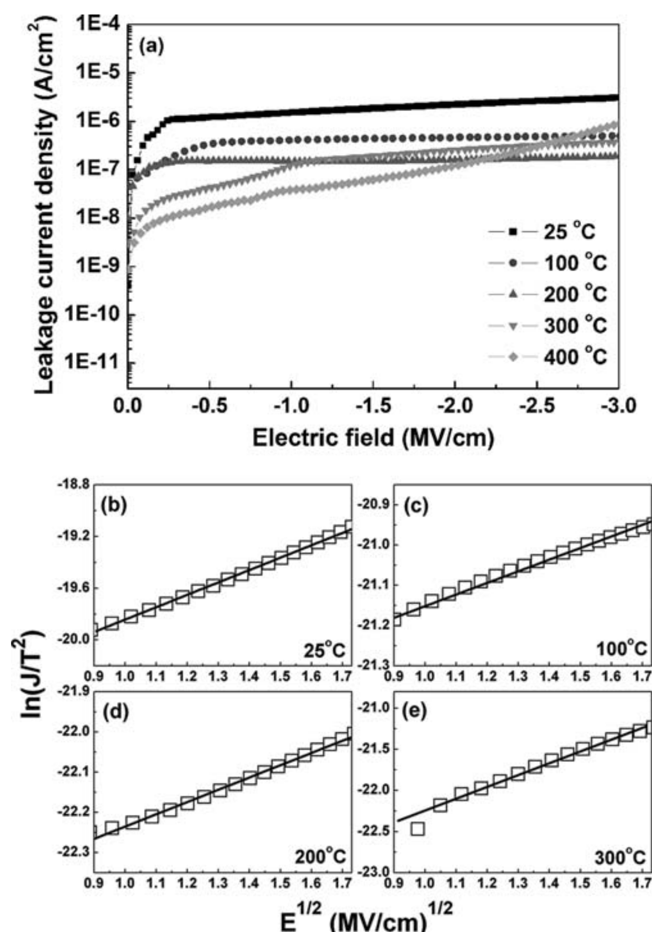


**Figure 8.** (a) The leakage current density versus electric field, and Schottky emission mechanism fitting, for the $SiC_xN_y$ films as a function of deposition temperature: (b) 25°C, (c) 100°C, (d) 200°C, and (e) 300°C.

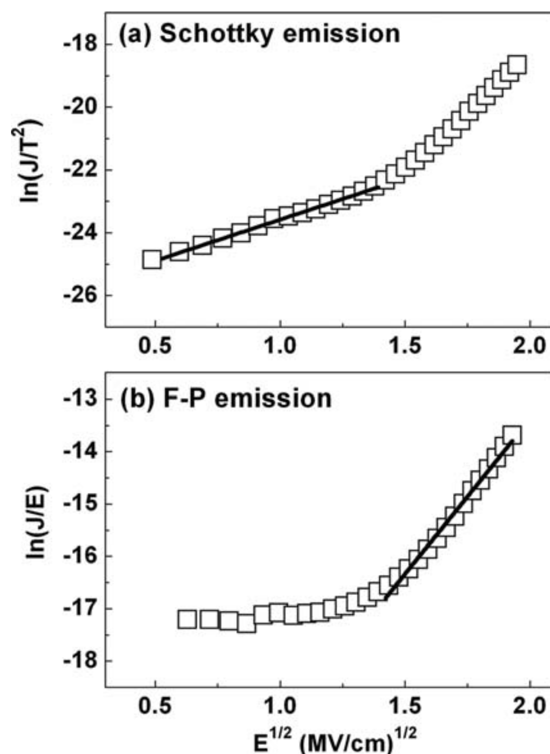


**Figure 9.** Conduction mechanism fitting of the $SiC_xN_y$ film deposited at 400°C: (a) Schottky emission and (b)Frenkel-Poole emission.

In comparison, F-P emission dominates the current conduction in the PECVD as-deposited $SiC_xN_y$ films using multi-precursors such as $SiH(CH_3)_3$+$NH_3$[14] or $Si(CH_3)_4$+$NH_3$.[31] Recently, Mallikarjunan et al.[32] demonstrates that the optimized carbon bonding in PECVD $SiC_xN_y$ film (plasma power density: 7.5–20 W/cm$^3$ if an electrode spacing of 1 mm is assumed) through the use of BASICN series of precursors with a combination of high Si–N and Si–C bond energies, is able to delay the onset of F-P emission. In our study of PECVD $SiC_xN_y$ films using a single precursor (VSZ), all films exhibited SE mechanism, except for the film deposited at 400°C, which was attributed to F-P emission mechanism under higher electric field. Our study showed that there are few charged defects in our $SiC_xN_y$ films, presumably due to less damage by using a cyclic precursor and a lower plasma power density of 0.15 W/cm$^3$.

The applicability of $SiC_xN_y$ in this study for the copper/low-k backend interconnects will be also examined and discussed in two critical areas: (1) resist poisoning and (2) etch selectivity. Resist poisoning is found to occur when basic contaminants, primarily amines in the as-deposited etch-stop films such as $SiC_xN_y$ using trimethylsilane+$NH_3$+He, diffuse into the photoresist and neutralize the photo-generated acids.[33] In comparison, our study is based on a single source precursor without $NH_3$ and operated at a low power density. We hypothesize that our $SiC_xN_y$ films will alleviate or eliminate the resist poisoning. Yet, this requires experimental validation in the patterning processes through the fabrication of multi-level copper/low-k test wafers in the future.

For the copper/low-k backend interconnects, a via-first patterning scheme has been widely used in a dual damascene integration process flow.[34,35] In the via etch process, highly selective etching of the low-k ILD against the underlying etch-stop layer, such as $SiC_xN_y$ in our case, is required. This is to ensure sufficient thickness of $SiC_xN_y$ film to protect the underlying copper layer from plasma induced damage and oxidation due to diffusion of oxygen. The etch selectivity requirement becomes more challenging as the low-k ILD is reduced to k < 2.6, which is achieved by incorporating high carbon content. Recently Kume et al.[35] reported that a high etch selectivity (∼10) can be achieved for a low-k ILD with high carbon content (C/Si = 2.7 for k = 2.55) against a $SiC_xN_y$ etch-stop layer with C/Si = 0.9 using $N_2$-Ar-$CF_x$ etching gas chemistry. In our study, as shown in Table II, a wide range of C/Si ratio from 0.29 to 1.82 was obtained with decreasing deposition temperature from 400°C to 25°C. We can infer that high etch selectivity can be achieved for our $SiC_xN_y$ films deposited at 100–300°C (C/Si = 0.72–0.81), and even higher for $SiC_xN_y$ film deposited at 400°C (C/Si = 0.29) if a low-k ILD with a high carbon content (C/Si ratio = 2.7) in Kume et al.'s study[35] is assumed. Even for $SiC_xN_y$ film deposited at room temperature (C/Si ratio = 1.82), a high selectivity is still possible by designing the etching gas chemistry to enhance their difference in etch rates of ILD and etch-stop layer with specific carbon contents.

## Conclusions

Low-k $SiC_xN_y$ films with k values of 3.6–4.6 were developed and prepared by RF PECVD (power density = 0.15 W/cm$^3$), at 25 to 400°C, using 1, 3, 5-trimethyl-1, 3, 5- trivinylcyclotrisilazane as a single precursor and Ar as the carrier gas. At lower deposition temperatures (≤200°C), the vinyl groups of the VSZ were broken and reformed to cross-linked Si-$(CH_2)_n$-Si linkages, during the plasma deposition process. However, most of the cyclic VSZ structures were preserved to create free volume in the $SiC_xN_y$ films, which resulted in a lower density (1.60–1.76 g/cm$^3$) and a lower dielectric constant (k∼3.6–3.9), with a fairly good elastic modulus of 22.0–25.0 GPa. When the deposition temperature was raised to ≥300°C, the cyclic N-Si-N linkages were broken up and reformed to a dense Si-N

Downloaded on 2014-04-28 to IP 140.113.38.11 address. Redistribution subject to ECS terms of use (see ecsdl.org/site/terms_use) unless CC License in place (see abstract).

structure, with the desorption of $CH_x$ bonds. This resulted in a higher density (1.8–2.0 g/cm$^3$) and a higher dielectric constant (4.2–4.6), with an excellent elastic modulus of 35.0–65.2 GPa. The leakage current density of $SiC_xN_y$ films was reduced from $1.5\times10^{-6}$ to 4.0 $\times10^{-8}$ A/cm$^2$ at 1 MV/cm, as deposition temperature was increased from 25°C to 400°C and their breakdown strengths were all >3 MV/cm. The conduction mechanism in all low-k $SiC_xN_y$ films was dominated by Schottky emission, except for the film deposited at 400°C, which was attributed to Frenkel-Poole emission mechanism under higher electric field. Our study showed that there are few charged defects in our $SiC_xN_y$ films, presumably due to less damage by using a cyclic precursor and a lower plasma power density of 0.15 W/cm$^3$. In summary, the $SiC_xN_y$ film deposited at 400°C had a fairly high elastic modulus of 65.0 GPa and a relatively low dielectric constant, k = 4.6. Moreover, it showed an excellent leakage current density, ~4.0 $\times10^{-8}$ A/cm$^2$ at 1 MV/cm and a high breakdown strength >3 MV/cm.

On the applicability of our $SiC_xN_y$ films in the copper/low-k backend interconnects, advantage and improvement are found in two critical areas: (1) resist poisoning and (2) etch selectivity. It is proposed that the use of a single source precursor and low plasma power density can alleviate or eliminate the resist poisoning, which required further experimental validation. Moreover, high etch selectivity can be achieved for our $SiC_xN_y$ films deposited at 100–300°C (C/Si = 0.72–0.81), and even higher for $SiC_xN_y$ film deposited at 400°C (C/Si = 0.29) if a low-k ILD with a high carbon content (C/Si ratio = 2.7) in Kume et al.'s study[35] is assumed.

## Acknowledgments

The authors are grateful for the financial support by National Science Council of ROC, under Contract Nos.: NSC 99-2221-E-009-177 and NSC 100-3113-E-007-002-.

## References

1. M. T. Bohr, *Solid State Technol.*, **39**, 105 (1996).
2. P. Gonon, A. Sylvestre, H. Meynen, and L. V. Cotthem, *J. Electrochem. Soc.*, **150**, F47 (2003).
3. A. S. Lee, N. Rajagopalan, M. Le, B. H. Kim, and H. M'Saad, *J. Electrochem. Soc.*, **151**, F7 (2004).
4. S. H. Rhee, M. D. Radwin, M. F. Ng, J. I. Martin, and D. Erb, *Appl. Phys. Lett.*, **83**, 2644 (2003).
5. M. A. Hussein and Jun He, *IEEE Trans. Semicond. Manuf.*, **18**, 69 (2005).
6. D. H. Zhang, L. Y. Yang, C. Y. Li, P. W. Lu, and P. D. Foo, *Thin Solid Films*, **504**, 235 (2006).
7. N. Chérault, G. Carlotti, N. Casanova, P. Gergaud, C. Goldberg, O. Thomas, and M. Verdier, *Microelectron. Eng.*, **82**, 368 (2005).
8. T. C. Wang, Y. L. Cheng, Y. L. Wang, T. E. Hsieh, G. J. Hwang, and C. F. Chen, *Thin Solid Films*, **498**, 36 (2006).
9. N. Fainer, Y. Rumyantsev, M. Kosinova, E. Maximovski, V. Kesler, V. Kirienko, and F. Kuznetsov, *Surf. Coat. Technol.*, **201**, 9269 (2007).
10. A. M. Wrobel, I. Blaszczyk-Lezak, A. Walkiewicz-Pietrzykowska, T. Aoki, and J. Kulpinski, *J. Electrochem. Soc.*, **155**, K66 (2008).
11. I. Martin, M. Vetter, A. Orpella, C. Voz, J. Puigdollers, and R. Alcubilla, *Appl. Phys. Lett.*, **81**, 4461 (2002).
12. S. M. Smith, T. Tighe, D. Convey, J. Quintero, and Y. Wei, *Thin Solid Films*, **516**, 885 (2008).
13. H. Cui and P. A. Burke, *J. Electrochem. Soc.*, **151**, G795 (2004).
14. C. W. Chen, T. C. Chang, P. T. Liu, T. M. Tsai, H. C. Huang, J. M. Chen, C. H. Tseng, C. C. Liu, and T. Y. Tseng, *Thin Solid Films*, **447–448**, 632 (2004).
15. E. Vassallo, A. Cremona, F. Ghezzi, F. Dellera, L. Laguardia, G. Ambrosone, and U. Coscia, *Appl. Surf. Sci.*, **252**, 7993 (2006).
16. A. M. Wrobel, I. Blaszczyk-Lezak, P. Uznanski, and B. Glebocki, *Chem. Vapor Depos.*, **16**, 211 (2010).
17. J. Lubguban, T. Rajagopalan, N. Mehta, B. Lahlouh, S. L. Simon, and S. Gangopadhyay, *J. Appl. Phys.*, **92**, 1033 (2002).
18. W. C. Oliver and G. M. Pharr, *J. Mater. Res.*, **7**, 1564 (1992).
19. A. M. Coclite, G. Ozaydin-Ince, F. Palumbo, A. Milella, and K. K. Gleason, *Plasma Process. Polym.*, **7**, 561 (2010).
20. Z. Chen, K. Prasad, C. Y. Li, S. S. Su, D. Gui, P. W. Lu, X. He, and S. Balakumar, *Thin Solid Films*, **462–463**, 223 (2004).
21. Y. Taki, T. Kitagawa, and Osamu Takai, *Thin Solid Films*, **304**, 183 (1997).
22. I. Ferreira, E. Fortunato, P. Vilarinho, A. S. Viana, A. R. Ramos, E. Alves, and R. Martins, *J. Non-Cryst. Solids*, **352**, 1361 (2006).
23. M. Tada, H. Yamamoto, F. Ito, T. Takeuchi, N. Furutake, and Y. Hayashi, *J. Electrochem. Soc.*, **154**, D354 (2007).
24. L. Favennec, V. Jousseaume, V. Rouessac, F. Fusalba, J. Durand, and G. Passemard, *Mater. Sci. Semicond. Process*, **7**, 277 (2004).
25. A. Zenasni, V. Jousseaume, P. Holliger, L. Favennec, O. Gourhant, P. Maury, and G. Gerbaud, *J. Appl. Phys.*, **102**, 094107 (2007).
26. C. Charles-Alfred and V. Jousseaume, *Surf. Coat. Technol.*, **201**, 9260 (2007).
27. Y. L. Cheng, J. Wu, T. J. Chiu, S. A. Chen, and Y. L. Wang, *J. Vac. Sci. Technol. B*, **29**, 031207 (2011).
28. S. M. Sze and K. K. Ng, *Physics of Semiconductor Devices*, John Wiley & Sons, New York (2007).
29. C. C. Chiang, I. H. Ko, M. C. Chen, Z. C. Wu, Y. C. Lu, S. M. Jang, and M. S. Liang, *J. Electrochem. Soc.*, **151**, G93 (2004).
30. J. Robertson and M. J. Powell, *Appl. Phys. Lett.*, **44**, 415 (1984).
31. K. Kobayashi, H. Yokoyama, and M. Endoh, *Appl. Surf. Sci.*, **254**, 6222 (2008).
32. A. Mallikarjunan, A. D. Johnson, L. Matz, R. N. Vrtis, A. Derecskei-Kovacs, X. Jiang, and M. Xiao, Microelectron. Eng., Available online 5 May 2011.
33. H. Nakao, S. Takei, T. Shinjo, and Y. Nakajima, *Advances in Resist Technology and Processing XXIII*, edited by Qinghuang Lin Proc. of SPIE Vol. 6153, 61532O, (2006).
34. T. Kropewnicki, K. Doan, B. Tang, and C. Björkman, *J. Vac. Sci. Technol. A*, **19**, 1384 (2001).
35. I. Kume, M. Ueki, N. Inoue, J. Kawahara, N. Ikarashi, N. Furutake, S. Saitoh, and Y. Hayashi, *Jpn. J. Appl. Phys.*, **50**, 04DB02 (2011).

Downloaded on 2014-04-28 to IP 140.113.38.11 address. Redistribution subject to ECS terms of use (see ecsdl.org/site/terms_use) unless CC License in place (see abstract).